Title

Cortical depth dependent population receptive field attraction by spatial attention in human V1

Authors

Barrie P. Klein[a], Alessio Fracasso[b,c,e], Jelle A. van Dijk[a,c], Chris L. E. Paffen[a], Susan F. te Pas[a], Serge O. Dumoulin[a,c,d]

[a] Experimental Psychology, Helmholtz Institute, Utrecht University, 3584 CS Utrecht, the Netherlands

[b] Radiology Department, University Medical Centre Utrecht, 3584 CX, Utrecht, the Netherlands

[c] Spinoza Centre for Neuroimaging, 1105 BK, Amsterdam, the Netherlands

[d] Experimental and Applied Psychology, VU University, 1081 HV, Amsterdam, the Netherlands

[e] Institute of Neuroscience and Psychology, University of Glasgow, Glasgow G12 8QB, UK

Corresponding author

Serge O. Dumoulin
s.dumoulin@spinozacentre.nl
Spinoza Centre for Neuroimaging
Meibergdreef 75
1105 BK Amsterdam
The Netherlands

Highlights (85 characters, including spaces, per point)

1. Voluntary spatial attention attracts population receptive fields (pRFs) in human V1
2. pRF attraction occurs throughout V1 and throughout the cortical thickness
3. pRF attraction is stronger near the gray/white matter boundary in V1
4. We suggest both feed forward and feedback processing underlie pRF attraction
5. We suggest that feedback signals arrive in deep cortical layers

Abstract

Visual spatial attention concentrates neural resources at the attended location. Recently, we demonstrated that voluntary spatial attention attracts population receptive fields (pRFs) toward its location throughout the visual hierarchy. Theoretically, both a feed forward or feedback mechanism could underlie pRF attraction at a given cortical area. Here, we use sub-millimeter ultra-high field functional MRI to measure pRF attraction across cortical depth and assess the contribution of feed forward and feedback signals to pRF attraction. In line with previous findings, we find consistent attraction of pRFs with voluntary spatial attention in V1. When assessed as a function of cortical depth, we found pRF attraction in every cortical portion (deep, center and superficial), although the attraction is strongest in deep cortical portions (near the gray white matter boundary). Following the organization of feed forward and feedback processing across V1, we speculate that a mixture of feed forward and feedback processing underlies pRF attraction in V1. Within this mechanism, the feedback component likely arrives in deep cortical portions.

Keywords

Spatial attention, Receptive field attraction, Sub-millimeter fMRI, attention field, population receptive field, visual cortex

1. Introduction

Visual attention is the mechanism through which we concentrate neural resources on relevant visual information. Computationally, the effects of visual attention on both human perception (Herrmann et al., 2010; Klein et al., 2016) and neural responses (Womelsdorf et al., 2008; Reynolds and Heeger, 2009; Klein et al., 2014) can be modeled as an interaction between two components, one representing the influence of attention (attention field) and the other representing a stimulus driven neural response property. Building on this attention field model, we have recently shown that visual attention voluntarily directed at a spatial location, attracts the population receptive fields (pRFs) towards the attended location across the visual hierarchy, producing distortions in the perceived location of visual stimuli (Dumoulin and Wandell, 2008; Klein et al., 2014, 2016).

Here, we examine the influence of voluntary spatial attention on pRF position across cortical depth in human V1. Imaging across cortical depth -or laminar imaging- may reveal unique information about the direction of information flow, specifically whether processes are driven by feed forward or feedback signals (Dumoulin et al., 2017; Lawrence et al., 2017; Self et al., 2017). In line with this notion, we recently showed that pRF size varies across cortical depth. This variation of pRF size across cortical depth closely resembles electrophysiological results and reflects the information flow across cortical depth (Fracasso et al., 2016; Self et al., 2017). Here we extend this approach to examine whether pRF attraction induced by attention varies across cortical depth in human V1.

We used ultra-high field (7T), sub-millimeter functional MRI (fMRI) to measure pRF position attraction as a function of cortical depth in V1. Using this approach, we first show that voluntary spatial attention attracts pRF preferred positions towards the attended location in V1. Furthermore, we find pRF attraction in every cortical portion, although the attraction is strongest near the gray/white matter boundary and decreases towards the cortical surface. Following the organization of feed forward and feedback afferent terminals in V1 (Hubel and Wiesel, 1972; Benevento and Rezak, 1976; Rockland and Pandya, 1979; Blasdel and Lund, 1983; Felleman and Van Essen, 1991), we speculate that a mixture of feed forward and feedback processing underlies pRF attraction in V1, with the feedback component likely arriving at depths close to the white matter.

2. Materials and Methods

2.1. Subjects

Twelve subjects participated in this study (three females, age range 21 - 42, mean age 28.6). All subjects had normal or corrected to normal visual acuity and gave informed consent. Two subjects were excluded from further analysis, one due to imaging artifacts and one to having an attention disorder. All experimental procedures were approved by the ethics committee of University Medical Center Utrecht.

2.2. Visual stimuli and experimental design

Visual stimuli were presented by back-projection onto a 15.0x7.9 cm screen inside the MRI bore. Subjects viewed the display through prisms and mirrors, and the total distance from the subjects' eyes (in the scanner) to the screen was 35.5 cm. Visible display resolution was 1024x538 pixels.

Stimuli were generated in Matlab using the PsychToolbox (Brainard, 1997; Pelli, 1997). The fixation cross was composed of two diagonal red lines covering the entire display, one pixel wide, intersecting at the center of the screen. Subjects were instructed to fixate the intersection of the two lines. This design facilitates accurate fixation (Schira et al., 2009). Stimuli consisted of a circular dartboard pattern presented behind the diagonal lines and centered on the center of the screen. The pattern consisted of 24 rings, each 0.24° visual angle wide. Each ring was divided into 12 black and white segments, each subtending 30°. The rings rotated around the center of the screen, moving at 60° per second. Neighboring rings moved in opposite directions.

The dartboard pattern was viewed through two C-shaped, equi-eccentric apertures. The apertures were centered on the horizontal meridian and subtended 120° each. The apertures were 0.86° visual angle wide and cycled through all eccentricities between 0.58° visual angle and 5.78° visual angle in 12 steps of 0.43° visual angle. On the last step in the stimulus cycle, the apertures were wrapped around the eccentricity range covering the inner most (0.58° visual angle - 1.01° visual angle) and outer most eccentricities (5.345° visual angle - 5.778° visual angle). This creates a cyclical stimulus that is assumed by our functional analysis (see section 2.7). The apertures only moved in the outward direction. Each step in the stimulus cycle lasted 4 seconds (1 TR, functional volume acquisition, see section 2.3). Consequently, one stimulus cycle lasted 48 seconds (12 TRs). One entire experimental run consisted of 6 stimulus repeats preceded by half a stimulus cycle to ensure a steady BOLD signal, totaling 78 TRs. We chose this specific stimulus as it allows us to estimate preferred eccentric position from the resulting BOLD signals using relatively little time points. This is necessary considering the slow repetition time (4 seconds) and limited number of time points per scan (72), which are typical for sub-millimeter functional imaging.

Simultaneous with the dartboard stimuli, we presented two circular $1/f$ noise patterns, 0.24° visual angle in radius. The noise patterns were centered

on the horizontal meridian, 6.3° visual angle left and right from fixation. The patterns randomly changed orientation every 250 ms and increased contrast on 5% of orientation changes (randomly chosen and different between functional scans; Figure 1).

Subjects were instructed to covertly attend one of the two noise patterns for the duration of one functional scan, and to detect contrast increments on the attended pattern. The attended location alternated between scans. The magnitude of the contrast increase was determined for each subject before scanning so that subjects found these increases difficult to detect but performed above chance (d' > 0). Regardless of the location that was to be attended, both noise patterns were always present and changed contrast independently. Subjects reported a contrast increment on the target on one side of the screen by a button press. They were instructed to ignore the other target on the other side of the screen. Prior to every scan, we indicated which target to attend via verbal instructions. We considered the detection of contrast increment correct if the subject responded within a 1 second window after the contrast increment on the attended side. Subjects performed above chance (d' = 2.05, SD = 0.32). We compared the performance of the attended target to the target on the other side. As this target was not attended, we assume this performance was driven by 'accidental hits'. This is confirmed by the detection rate (d' = 0.81, SD = 0.24), which was significantly worse than for the attended target ($t = 24.4$, $p < 0.001$, two-sided, paired samples t-test). We found no differences between performance for the left and right targets ($p = 0.88$, two-sided, paired samples t-test). The above analysis confirms that subjects were attending the intended target and ignoring the target on the other side.

Figure 1

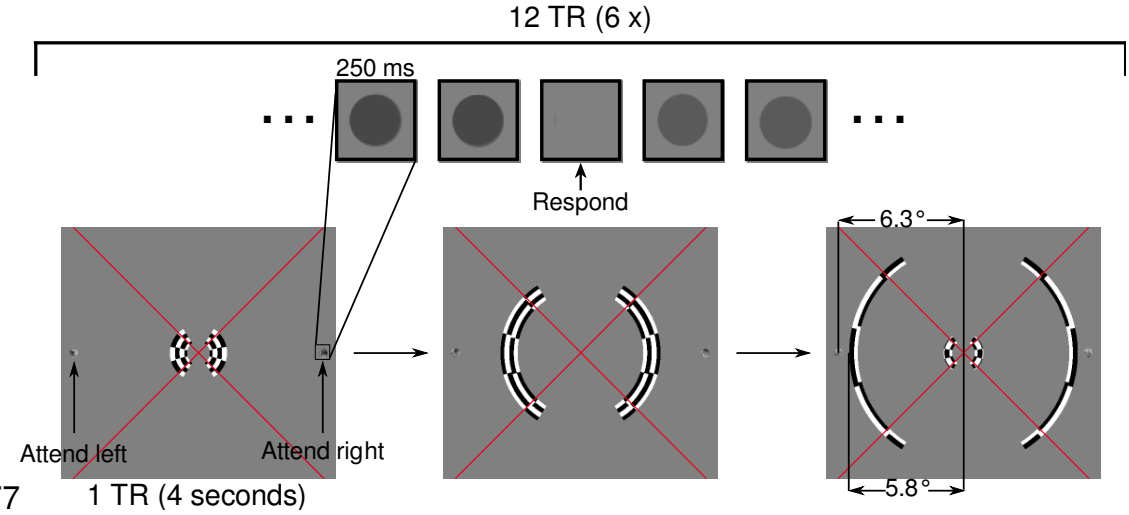

Figure 1. Stimulus and task. Subjects fixated the center of the screen, marked by the intersection of two diagonal red lines running across the screen. The stimulus consisted of a rotating dartboard pattern viewed through two C-shaped apertures. The apertures moved from the center of the screen towards the periphery in an expanding fashion. One stimulus cycle lasted 12 TRs (1 TR = 4 seconds) and was repeated 6 times during one functional scan. Concurrently, we presented two 1/f noise patterns left and right of the center of the screen. The noise patterns changed orientation independently every 250 ms and increased in contrast on 5% of orientation changes. Subjects were instructed to covertly attend either the left or right noise pattern for the duration of one functional scan and report the contrast increments of the attended pattern.

2.3. Functional data acquisition

High resolution functional data were acquired using a Philips 7T scanner (Best, Netherlands) and a volume transmit coil for excitation (Nova Medical, MA, USA). Head motion inside the scanner was minimized using a combination of noise-cancelling headphones and foam padding. Functional T2*-weighted 3-dimensional multi-shot EPI (3D-EPI, two shots per slice, 35 slices, 70 shots overall) data were acquired using two custom-built high-density 16-channel surface coils with a of total 32 channels for signal reception (Petridou et al., 2013). The sequence parameters were: TR/TE = 57/28 ms, flip angle: 20°, acceleration factor using SENSE encoding: 3.5 (right-left) × 1.3 (anterior-posterior), echo planar factor: 27, BW (phase-encode): 19.1 Hz/pixel, readout duration ~ 52 ms (with potential blurring in the phase-encode direction estimated at ~ 16%; Haacke et al.,1999), voxel size = 0.70 mm isotropic, FOV = 131 (right-left) × 120 (feet-head) × 24.5 (anterior-posterior) mm^3, 35 coronal slices, and 28% oversampling in the slice direction. This acquisition sequence produced geometric distortions near the edges of the functional imaging volume. Furthermore, distortions are more severe near the air/tissue interface, for example near the edge of cortical gray matter (Truong et al., 2008), and near the basal ganglia due to B0 inhomogeneities resulting from iron storage. By limiting our analyses to primary visual cortex (the calcarine sulcus) we attenuate the effects of geometric distortions in our functional data, as it is away from the edges of the cortical gray matter and basal ganglia. We centered the functional volume on the calcarine sulcus to place it away from the distortions near the edges of the functional volume and minimize their effect on our functional data. Functional volumes were acquired every 4 s, and functional scans were each 312 s (78 functional acquisitions) in duration. Each subject completed 6 to 8 functional runs in a single session.

2.4. Anatomical data acquisition and processing

For five subjects (S1, S3, S6, S7, S10) anatomical images were acquired using a 3D T1-weighted MPRAGE sequence (TR = 7.48 ms, TE = 3.47 ms, flip angle = 8°, FOV: 250 x 200 x 180 mm, voxel size 0.5 x 0.5 x 0.5 mm). For two subjects (S2 and S9) anatomical T1-weighted images were acquired using the MP2RAGE sequence (Marques et al., 2010) with the following parameters: TR = 5982 ms, FOV: 220 x 220 x164 mm, voxel size: 0.625 x 0.625 x 0.64 mm, TI1/TI2 = 800/3686 ms, flip angle = 7°/5°. For two subjects (S4 and S8), T1-weighted images were acquired at a resolution of 0.5x0.5x0.8 mm (TR = 7ms, TE = 2.84 ms, flip angle = 8°). All the above anatomical images were acquired on a Philips 7T scanner using a 32-channel head coil. Finally, for one subject (S5), T1-weighted images were acquired on a Philips 3T scanner (TR 10.029 ms TE = 4.6 ms, flip angle = 8°, voxel size 0.75 x 0.75 x 0.8 mm). Anatomical images not acquired at 0.5 mm isotropic resolution were resampled to this resolution. Gray/white matter segmentations were obtained in MIPAV using the TOADS/CRUISE algorithm (Han et al., 2004; Bazin and Pham, 2007) and subsequently manually corrected. We

employed the equi-volume model approach to build a coordinate system along cortical depth taking local curvature into account (Waehnert et al., 2014).

2.5. V1 ROI definitions

V1 definitions were acquired during separate scanning sessions, or for the purposes of a different experiment. In both cases, we used a regular pRF mapping stimulus, described in detail by Dumoulin and Wandell (2008). In summary, this stimulus consisted of a contrast defined, bar shaped checkerboard pattern moving across the visual field in eight different directions (four cardinal, four diagonal). We used a regular pRF modeling procedure (Dumoulin and Wandell, 2008) to estimate each voxel's best fitting pRF as described by its position in the visual field (X and Y) and its extent (standard deviation, sigma). We converted the X and Y positions of every pRF to polar angle and eccentricity estimates, which were rendered on an inflated cortical surface (Wandell et al., 2000). The position of V1 was obtained by following reversals in polar angle and eccentricity progressions (Sereno et al., 1995; Wandell et al., 2007). V1 ROI definitions were imported into the subject's high-resolution anatomical space. Finally, we clipped V1 ROI definitions to account for differences in the polar angle and eccentricity coverage between the pRF mapping stimuli used to define V1 and the current experimental stimulus.

2.6.Pre-processing of functional data

Functional data was preprocessed using AFNI (Cox, 1996). We corrected for head motion between scans by aligning the first functional volumes for each scan using 3dvolreg. Correction for within-scan motion was done by aligning all the frames of a run to the first frame. We corrected for between and within-scan motion in a single step and averaged the motion corrected images from a single session together. We coregistered the averaged functional image to the motion-corrected and averaged T1 weighted image using an affine transformation. The coregistration was divided into three steps. First, we clipped the T1-weighted anatomy in the anterior-posterior direction, leaving only the occipital lobe. As we used different receive coils for our functional and anatomical data acquisition, we obtained a good starting point for the coregistration by centering the functional image on the clipped anatomy using their respective centers of mass of the reduced FOV volumes, or manually using 3dSlicer (http://www.slicer.org; Fedorov et al., 2012). Second, the averaged functional image was coregistered with the T1 weighted images using an affine transformation via the function 3dAllineate, using the two-pass option. This procedure blurs the functional image and initially allows for a large rotation and shift, and then refines the coregistration using an affine transformation. In the third step the resulting coregistration was further optimized via 3dAllineate, but now using the one-pass option. This does not blur the functional image and thus coregisters the original functional volume with the anatomy. It allows only for a small amount of motion, again using an

affine transformation. The obtained transformations were combined in a single affine transformation matrix.

We used local Pearson correlation as the cost function for our coregistration (Saad et al., 2009) but adopted alternative cost functions (such as mutual information and normalized mutual information) when this initial cost function yielded unsatisfactory results. Our main priority was to obtain an optimal coregistration around the calcarine sulcus. Coregistration output was visually inspected by evaluating the location of anatomical markers as gray matter / white matter (GM/WM) and gray matter/cerebrospinal fluid (GM/CSF) boundaries in the calcarine sulcus, and by the correspondence of the position of large vessels between the T1-weighted and the averaged functional data.

2.7. Functional and statistical analysis

We discarded the first six volumes of every functional run and averaged the functional scans for both conditions (attend left / attend right) separately. We parameterized the fMRI time series using the traveling wave analysis implemented in the mrVista software package for Matlab (http://white.stanford.edu/software; Engel et al., 1994; Engel, Glover, & Wandell, 1997; Sereno et al., 1995). This analysis yields three parameters: phase, amplitude and coherence. The phase gives the temporal delay of the stimulus frequency in the time series in radians. Within our stimulus design, this is a measure of preferred eccentric position. The amplitude gives the BOLD amplitude in percentage signal change at the stimulus frequency. Finally, coherence is the correlation between the harmonic at the stimulus frequency and the fMRI time series. As such, it is a measure of signal quality and reliability of the corresponding phase value. Finally, we interpolated these parameters into the anatomical space, using nearest neighbor interpolation and the transformation computed during the coregistration (see section 2.6).

We measured the phase for every voxel in the functional volume twice, once while attention was directed at the hemifield ipsilateral to the voxel (ipsilateral hemisphere) and once while attention was directed at the hemifield contralateral to the voxel (contralateral hemisphere). We computed pRF attraction between conditions by subtracting the phase estimate measured for a voxel when it was located in the hemisphere ipsilateral to the attended target, from the phase estimate for the same voxel when it was located in the hemisphere contralateral to the attended target. These phase differences were wrapped to yield values ranging from -pi to pi, with positive values corresponding to higher preferred eccentric positions in the attended hemifield. Next, we converted the phase differences to degrees of visual angle by dividing by 2pi and multiplied them by the stimulus range (5.2° visual angle), yielding preferred eccentric position changes in degrees visual angle. We excluded anatomical voxels outside V1 (see section 2.5) and those that were located outside the gray matter. Also, we excluded voxels with a coherence value lower than the 25th percentile in either one of the conditions. Additionally, to reject voxels with pRFs near the stimulus edge, we excluded

voxels with an averaged phase of less than the 12.5th percentile or more than the 87.5th percentile of the stimulus eccentricities.

We assessed the statistical significance of the preferred eccentric position changes (Figure 3D) across V1 using paired samples t-tests. These t-tests were performed using anatomical voxels as individual data points. As the spatial resolution of the anatomical volumes is higher than the spatial resolution of the functional volumes, the functional volumes were upsampled to match the anatomical resolution. The t-tests reported were corrected for this upsampling. We assessed the variation of the preferred eccentric position changes across cortical depth for both the attention conditions (Figure 4E), eye movement control data, and a simulation (Figure 5B), using linear regression. Similarly, we analyzed the increase in fMRI response amplitude (Figure 4D) and change in fMRI response amplitude between conditions (Figure 6A) as a function of cortical depth, using linear regression. These linear regression analyses used the binned averages for all subjects together as its individual data points. The linear regression weighted the binned averages by the number of voxels each average represents.

2.8. Averaged BOLD responses (Figure 3C)

To assess differences in BOLD responses, we only included fMRI time series corresponding to voxels included in the phase analysis (see section 2.7). We averaged the BOLD responses to all stimulus repeats together, giving the averaged BOLD response to a single stimulus cycle. Next, we used linear interpolation to align the BOLD responses according to their averaged phase across the two conditions. Finally, we averaged the aligned BOLD responses from all voxels together, separately for when attention was directed at the target in the contralateral and ipsilateral hemifield. Conceptually, this analysis yields the averaged BOLD response from both conditions in the hypothetical case that all pRFs in V1 have the same preferred eccentric position when averaged across conditions.

2.9 Hypothesized profiles of pRF attraction across cortical depth

To hypothesize how contributions of feed forward and feedback processing to pRF attraction may shape the profile of pRF attraction across cortical depth, we combined an attention field model with the known functional and anatomical organization of laminar connectivity (Hubel and Wiesel, 1974; Felleman and Van Essen, 1991; Fracasso et al., 2016; Dumoulin et al., 2017). In this section, we first apply an attention field model to our experimental design. Then we discuss how the forward flow of signals across cortical depth affects pRF properties in V1. Finally, we consider how this flow will shape the profile of pRF attraction across cortical depth.

2.9.1. Attention field model. As we summarize the fMRI responses using one parameter, eccentricity, we consider the pRFs underlying the fMRI responses to be a one dimensional Gaussian defined along the radial axis (x) (Dumoulin and Wandell, 2008; Fracasso et al., 2016):

374
375 Equation 1

$$\int_{R} p\,F(x) \cdot e^{-\frac{(x-\mu_{pRF})^2}{2\sigma_{pRF}^2}}$$

376
377where μ_{pRF} is the preferred eccentric position and σ_{pRF} is the size (standard
378deviation) of the pRF. We model the effect of attention on preferred eccentric
379position as a multiplication between two Gaussians (Womelsdorf et al., 2008;
380Reynolds and Heeger, 2009; Klein et al., 2014). One of these represents the
381influence of attention -the attention field- whereas the other represents the
382pRF without the influence of attention; the stimulus driven pRF. This
383multiplication produces a third Gaussian, representing the pRF under
384influence of attention. As such, the preferred eccentric position of the pRF
385under attention ($\mu_{AF\times pRF}$) is given by:
386

$$\mu_{AF\times pRF} = \frac{\mu_{AF}\sigma_{pRF}^2 + \mu_{pRF}\sigma_{AF}^2}{\sigma_{AF}^2 + \sigma_{pRF}^2}$$

387 Equation 2
388
389where μ_{AF} and μ_{pRF} represent the positions and σ_{AF} and σ_{pRF} the sizes of
390the attention field and stimulus driven pRF. Importantly, we compare the
391preferred eccentric position under two different conditions. Consequently, the
392preferred eccentric position change between the two conditions is given by:
393

$$\mu_{AFr\times pRF} - \mu_{AFl\times pRF} = \left[\frac{\mu_{pRF}\sigma_{AFr}^2 + \mu_{AFl}\sigma_{pRF}^2}{\sigma_{AFr}^2 + \sigma_{pRF}^2}\right] - \left[\frac{\mu_{pRF}\sigma_{AFl}^2 + \mu_{AFl}\sigma_{pRF}^2}{\sigma_{AFl}^2 + \sigma_{pRF}^2}\right]$$

394 Equation 3
395
396We assume that the stimulus driven pRF sizes are the same for both
397conditions. Moreover, the voluntary attention task was performed on targets
398with identical properties and performance was similar for both conditions.
399Therefore, we also assume the attention field sizes to be similar between the
400two conditions ($\sigma_{AFr} = \sigma_{AFl}$). Finally, as the attended targets are at the same
401distance from fixation, the attention fields in both conditions are the same
402distance from fixation as well($\mu_{AFr} = -\mu_{AFl}$). Under these assumptions,
403Equation 3 can be simplified to:
404

$$\Delta\mu_{AF} = \frac{(\mu_{AFr} - \mu_{AFl})\sigma_{pRF}^2}{\sigma_{AF}^2 + \sigma_{pRF}^2}$$

405 Equation 4
406
407As such, this model predicts that preferred eccentric position changes ($\Delta\mu_{AF}$)
408are a function of the attention field size, stimulus driven pRF size and the
409distance between the two attended locations ($\mu_{AFr} - \mu_{AFr}$). Because of our

experimental design, the attention field size and distance between attended locations are the same for every pRF: only the pRF size will vary across pRFs. Therefore pRF size will be the major source of variation in preferred eccentric position changes in our design (Klein et al., 2014).

2.9.2. Forward flow across cortical depth. Within the context of V1's neural organization, we assumed that the stimulus driven size and preferred eccentric position of the pRF (without the effect of attention) are the result of feed forward processing. Regarding V1, these feed forward signals predominantly originate in the lateral geniculate nucleus (LGN) and terminate in V1's central cortical depths (Figure 2A, pRF; Blasdel & Lund, 1983; Callaway, 1998; Felleman & Van Essen, 1991; Hubel & Wiesel, 1972). Subsequently, neural populations in deep and superficial cortical portions inherit their feed forward, stimulus driven pRFs by sampling from neural populations in central cortical portions (Figure 2A, pRF';Briggs & Callaway, 2001; Callaway, 1998; Fitzpatrick, Lund, & Blasdel, 1985; Fracasso et al., 2016; Maunsell & Gibson, 1992; Self, Kerkoerle, Supèr, & Roelfsema, 2013; Usrey & Fitzpatrick, 1996; Yoshioka, Levitt, & Lund, 1994).

One way to model sampling from one cortical layer to another is as a convolution, where a single neural population in deep and superficial cortical portions receives input from multiple populations in the central cortical portion (Fracasso et al., 2016). This way, the properties of pRFs in deep and superficial cortical portions can be obtained by convolving a function representing the response property at central cortical portions (a pRF Gaussian in this case) and a function representing the sampling function. Between visual field maps, this sampling function is Gaussian shaped (Motter, 2009; Kumano and Uka, 2010; Harvey and Dumoulin, 2011; Haak et al., 2013) and this approach was recently extended to sampling between layers (Fracasso et al., 2016). As such, pRFs in deep and superficial cortical portions are the product of the convolution between two Gaussian functions, one representing the pRF at central cortical portions and one representing the sampling function from this cortical portion.

Conceptualizing sampling between cortical layers this way highlights two important points: (1) pRF sizes will increase from central to deep and superficial cortical portions (Fracasso et al., 2016) and (2) the pRF position of a neural population in the deep or superficial cortical portion is equal to the Gaussian weighted average of the positions of the pRFs this population samples from the central cortical portion (Fracasso et al., 2016). In other words: sampling between cortical portions does not change pRF positions between cortical portions (Figure 2A, $\mu'_{pRF} = \mu_{pRF}$)(Hubel and Wiesel, 1974). In summary, the feed forward flow of information produces larger pRF sizes in deep and superficial cortical portions (Fracasso et al., 2016) but no systematic variation of pRF position across cortical depth.

2.9.3. Attention field model applied to information flow across cortical depth. When applied to feed forward processing in V1, the attention field represents

an attentional influence that produces pRF attraction by interacting with feed forward input to V1 via, for example, response modulation at the level of the LGN (McAdams and Maunsell, 1999; O'Connor et al., 2002; Compte and Wang, 2006; McAlonan et al., 2008). As feed forward input to V1 terminates in central cortical portions, we can model pRF attraction in a feed forward process as an interaction between the attention field and the stimulus driven pRF in V1's central cortical portion (Equation 4; Figure 2B, AF x RF). As discussed above, this attracted pRF position in the central cortical portion will be inherited by the deep and superficial cortical portions (Figure 2B, pRF'_{AF}). Thus unlike our speculations in an earlier paper (Klein et al., 2014), sampling between cortical layers as modeled here cannot amplify pRF attraction. In other words, feed forward information flow will inherit the pRF attraction from central layers and is in this case not a fraction of pRF size. Thus, we hypothesize that a feed forward-driven pRF attraction yields a uniform pRF attraction across cortical depth (Figure 2D).

When applied to feedback processing, the attention field represents an attentional influence that is fed back to V1, where it interacts with feed forward, stimulus driven processing to produce pRF attraction (Figure 2C; Compte and Wang, 2006; Bobier et al., 2014). Feedback connections terminate specifically in deep and superficial portions in V1 (Lund et al., 1975; Benevento and Rezak, 1976; Rockland and Pandya, 1979; Felleman and Van Essen, 1991; Yoshioka et al., 1994; Shipp, 2003). As such, the interaction between the attention field and stimulus driven pRF will specifically occur in deep and/or superficial cortical portions akin to equation 4 (Figure 2C, green and blue arrows respectively). Thus, we hypothesize that a feedback driven pRF attraction yields a non-uniform pRF attraction across cortical depth, specifically with larger attraction at deep and/or superficial depths (Figure 2E).

In conclusion, we have highlighted several important concepts. (1) Within our design, pRF attraction will be a function of pRF size. (2) Feed forward hierarchical sampling will not increase pRF attraction (3) If attention attracts pRFs in V1 via a feed forward process, this attraction will be the same (inherited) across cortical depth. (4) If attention attracts pRFs in V1 via a feedback process, this will happen via feedback afferents in deep and superficial cortical portions yielding (stronger) pRF attraction limited to deep or superficial cortical portion, or both.

Figure 2

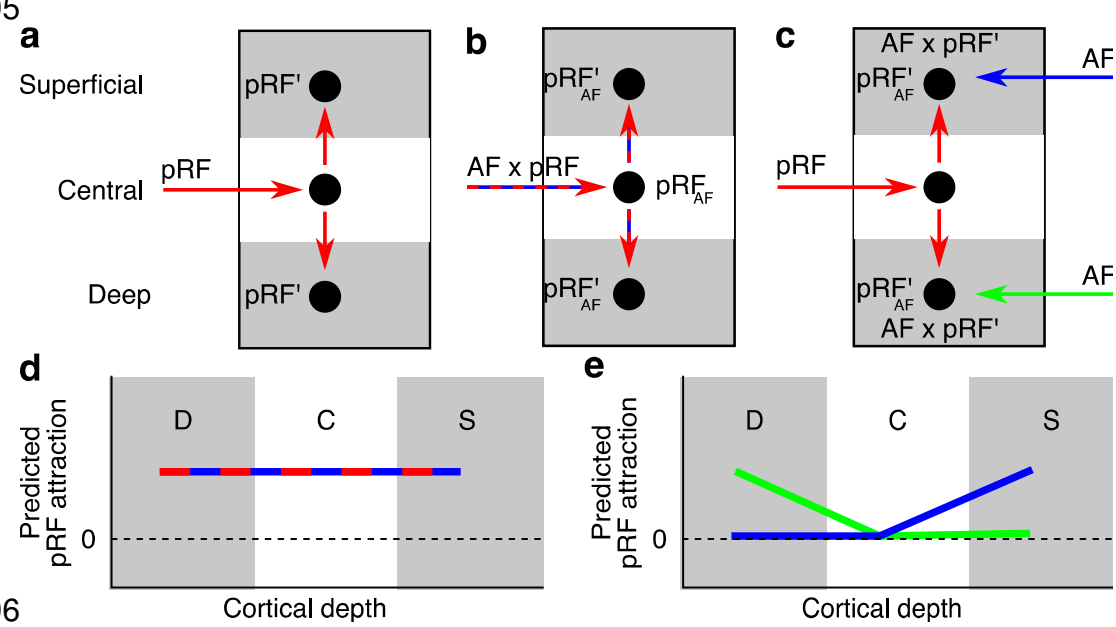

Figure 2 Hypothesized profiles of pRF attraction across cortical depth. a. Neural populations in the central cortical portion obtain their pRFs through forward inputs from the lateral geniculate nucleus (LGN; red horizontal arrow). Following the forward flow of information across cortical depth, neural populations in deep and superficial cortical portions sample from the central cortical portion (pRF', red vertical arrows), resulting in larger pRF sizes, but identical pRF positions (Fracasso et al., 2016). **b.** We model a feed forward mechanisms of pRF attraction as an interaction between the attention field (AF) and the stimulus driven pRF in the central cortical portion (AF x pRF). This produces the pRF under influence of attention in the central cortical portion (pRF_{AF}), with a pRF position attracted towards the attended location. Through sampling from central cortical portions, neural populations inherit their pRFs (pRF'_{AF}), yielding larger pRF sizes but identical pRF positions. Thus pRF attraction will be constant across cortical depth and not co-vary with pRF size. **c.** We model a feedback implementation of pRF attraction as an interaction between the attention field and pRFs in deep and superficial cortical portions (AF x pRF', blue and green arrow). This produces pRFs under influence of attention in deep and superficial cortical portions (pRF'_{AF}). We speculate that this interaction may occur either in both deep and superficial cortical portions, or can be limited to the deep or superficial portion only. Thus, pRF attraction will increase in deeper and/or superficial portions. **d.** A feed forward implementation of pRF attraction (b) predicts no variation of pRF attraction across cortical depth, as deeper and superficial layers inherit the pRF attraction from central cortical depths. This prediction dissociates pRF size from pRF attraction. **e.** A feedback implementation of pRF attraction (c) predicts that pRF attraction specifically occurs in either deep or superficial cortical depths, or both.

2.10. *Eye movement controls*

Prior to the scanning sessions, we trained subjects on the experimental task outside the scanner while we monitored their eye movements using a highly accurate, head mounted Eyelink II system (SR Research). To estimate the bias in gaze position towards the attended targets, we subtracted the median gaze position during the attend left condition from the median gaze position during the attend right condition for every subject separately. Averaged across subjects, the median gaze position difference per condition was 0.046° visual angle, yielding a total bias between conditions of approximately 0.092° visual angle.

For this control experiment, we presented the same stimulus in the scanner as in the main experiment (Figure 1), but we shifted the fixation cross 0.1° visual angle to the left or right relative to the center of the stimulus, alternating left and right fixations between scans. This yields a gaze position difference between conditions of 0.2° visual angle, which is twice the size of the average bias in gaze position measured prior to scanning sessions. For this control experiment, the color of the fixation cross alternated between red and green and subjects had to report the color changes and ignore the targets left and right of the stimulus. We analyzed the data from this experiment in the same way as the data from the main experiment (see sections 2.6 and 2.7).

As the averaged bias in gaze position is less than the average main effect on preferred eccentric position change, we also generated a simulated data set with an eye movement bias scaled to match the size of the average preferred eccentric position change in the main experiment. As eye movements towards (or away from) the attended location move pRFs to higher (or lower) eccentricities, they are stimulated later (or earlier) by our stimulus. In order to simulate a larger bias in the BOLD time series measured for the eye movement control experiment, we interpolated the BOLD time series to later time points in the hemispheres contralateral to the direction of the fixation shift (i.e. right (or left) hemisphere when the fixation cross is shifted to the left (or right)), and to earlier time points in the hemispheres ipsilateral to the fixation offset.

We determined the amount of interpolation for every TR separately by random sampling from the distribution of gaze positions measured for each subject, adding or subtracting a fixed amount to produce the desired average offset between the two conditions. Doing so, we created 1000 data sets for every subject in the eye movement control condition with an eye movement offset between the two conditions, that, on average, matched the attentional effect observed in the main experiment. As we sampled from the subject's distribution of gaze positions from pre-scanning sessions, the shift variance was matched to the subject's gaze position variance.

3. Results

3.1. pRFs in V1 are attracted toward the locus of spatial attention

Inside the MRI scanner, subjects fixated the center of the screen while they performed an attention demanding contrast discrimination task at 6.3° left or right from fixation, for the duration of one functional scan (Figure 1). Following the attention field model (Womelsdorf et al., 2008; Reynolds and Heeger, 2009), we predicted that voluntary attention to either target would result in pRF attraction towards the attended target (Klein et al., 2014). Importantly, this attraction would manifest as higher preferred eccentric positions for pRFs near the horizontal meridian in the hemifield containing the attended location.

To examine preferred eccentric positions near the horizontal meridian during task performance, we measured fMRI responses to two equi-eccentric, C-shaped, dartboard stimuli. The dartboard stimuli moved in a traveling wave design (Engel et al., 1994; Fracasso, Petridou, & Dumoulin, 2016; Sereno et al., 1995), i.e. from the fixation point towards the attended location, up to 5.8°, in an expanding fashion. By using C-shaped stimuli we limited visual stimulation to around the horizontal meridian (Figure 1). One functional scan consisted of six stimulus repetitions, producing six peaks in each voxel's fMRI response, which correspond to the stimulus passing through its pRF six times (Figure 3A).

We extracted preferred eccentric positions from the fMRI responses from the attend left and attend right condition separately and assessed the quality of these estimates by overlaying them on a reconstructed cortical surface. As expected, preferred eccentric positions gradually increased along the posterior - anterior axis for both conditions and for all subjects (Figure 3B, see Supplemental Figure 1 for all subjects). As can be seen from Figure 3B, the preferred eccentric positions changed between the two conditions (highlighted by the solid black lines). More specifically, in the left hemisphere, the preferred eccentric positions were higher during the attend right condition (Figure 3B, upper panel) than those during the attend left condition for the same voxels (3B, lower panel).

We averaged the fMRI responses underlying the preferred eccentric positions from the hemispheres contralateral to the attended target (i.e. left and right hemispheres for the attend right and attend left conditions respectively) and ipsilateral to the attended target (i.e. right and left hemispheres for the attend right and attend left conditions respectively; Figure 3C). This revealed that the responses from the contralateral hemispheres were delayed compared to those from the ipsilateral hemispheres. As the stimuli covered higher eccentricities at later time points in the sequence, this delay corresponded to an increase in preferred eccentric position in the hemifield containing the attended target, demonstrating pRF attraction towards the attended target.

We quantified this pRF attraction for every voxel in V1. We measured preferred eccentric positions for every voxel twice, once when it was located in the hemisphere contralateral to the attended target (e.g. attend left for right

hemisphere voxels) and once when it was located in the hemisphere ipsilateral to the attended target (e.g. attend right for right hemisphere voxels). We subtracted the preferred eccentric positions measured in the ipsilateral hemispheres from those measured in the contralateral hemispheres to give the preferred eccentric position change between the two conditions, which measures pRF attraction towards the attended targets for every voxel. This revealed a significant increase in preferred eccentric position in the contralateral hemispheres for every subject separately (Figure 3D, two-sided, paired samples t-test, all p values < 0.001). These preferred eccentric position changes demonstrate that across V1, voluntary spatial attention attracts pRFs towards its location, as predicted by attention field models.

FIGURE 3

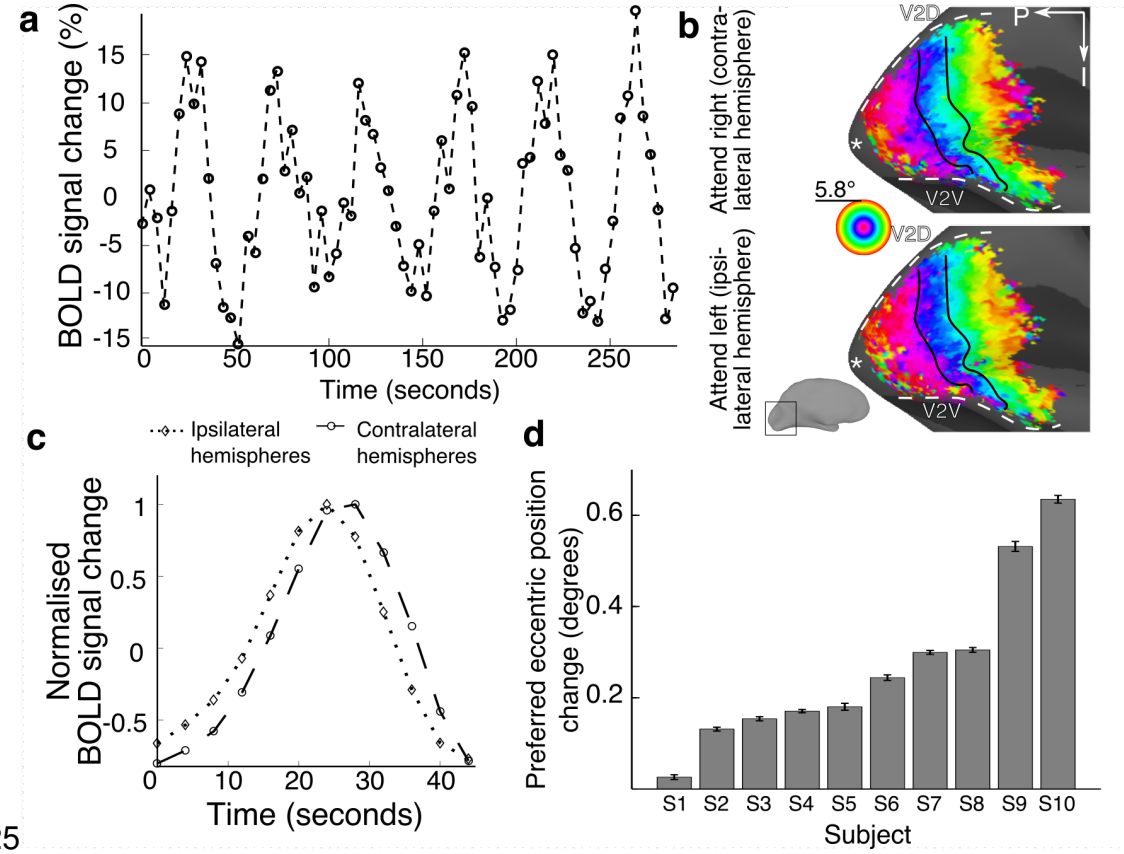

Figure 3. Preferred eccentric position changes across V1. **a.** fMRI response from one condition and one cortical location (voxel of 0.68x0.68x0.70mm). We measured six peaks in the fMRI response, corresponding to the six stimulus cycles. **b.** Preferred eccentric positions from V1 overlaid on a reconstructed cortical surface of the left hemisphere (inset), for the attend right (upper panel, contralateral hemisphere) and the attend left (lower panel, ipsilateral hemisphere) conditions. Preferred eccentric positions change between the two conditions, as illustrated by identical iso-eccentric solid black lines). White dashed lines mark the boundary between V1 and V2 ventral (V2v) and V2 dorsal (V2d). The white asterisk marks the foveal representation. The arrows indicate the posterior - anterior (P) and superior - inferior (S) axis. **c.** Average fMRI responses from V1 of one subject averaged across stimulus cycles. Responses differ depending on whether the attended location was ipsilateral (dotted line and diamonds) or contralateral (dashed line and circles). Specifically, the delay of the fMRI responses differs, which is interpreted as different preferred eccentric positions. **d.** The average V1 preferred eccentric position change between the two conditions in degrees visual angle for every subject. Every subject had a significant preferred eccentric position change between the two conditions corresponding to a pRF attraction towards the attended targets. Subjects are sorted by the size of their preferred eccentric position change. Error bars represent the standard errors of the mean.

3.2. pRF attraction in V1 is strongest in the deep cortical portion

We hypothesized that feed forward and feedback signals may produce different profiles of preferred eccentric position change across cortical depth in V1 (see section 2.9; Figure 2). In short, we speculated that if pRF attraction is driven by feed forward signals, this would yield no systematical variation of preferred eccentric position change across cortical depth. If, however, pRF attraction is driven by feedback signals, we would measure stronger preferred eccentric position changes in either deep cortical portions or superficial cortical portions, or both.

We assessed how changes in preferred eccentric position, measuring pRF attraction towards the attended targets, varied across cortical depth in V1. To this end, we acquired high-resolution anatomical images for every subject and computed equi-volume estimates of normalized cortical depth (Waehnert et al., 2014; Figure 4A and B and Supplemental Figure 1). Next we imported the estimated preferred eccentric positions (Figure 4C and Supplemental Figure 1) and fMRI response amplitude for both conditions into the anatomical space (see sections 2.6 and 2.7).

We first verified our methods by examining the variation in fMRI response amplitude across cortical depth. As we used a 3D gradient echo (GE) sequence, we should find an increase in fMRI response amplitude towards the cortical surface (De Martino et al., 2013; Duvernoy, Delon, & Vannson, 1981).

For each subject separately, we divided the depth estimates into ten equally sized bins and computed the averaged fMRI response amplitude for each bin for the contralateral and ipsilateral hemispheres separately and averaged across subjects subsequently. As expected, the fMRI response amplitude increased towards the cortical surface for both conditions, confirming the validity of our methods and data (Figure 4D and Supplemental Figure 1). Note that the increase in response amplitude differed between contralateral and ipsilateral hemispheres. We will address differences in fMRI response amplitude in detail below.

Next, we assessed how pRF attraction varied across cortical depth. Again, we divided the depth estimates into ten equally sized bins and computed the averaged preferred eccentric position change per bin for every subject separately (Supplemental Figure 1). To average all subjects together, we subtracted each subject's mean pRF attraction (Figure 3D). We then averaged across all subjects together, weighting each subject's data by the number of voxels they contributed, and added the mean pRF attraction across all subjects to the averaged binned data (Figure 4E). For all subjects combined, we found a significant negative slope of the binned preferred eccentric position changes across cortical depth (weighted linear regression, slope coefficient = -0.070 degrees of visual angle, $p < 0.001$). Given an averaged preferred eccentric position change across V1 of 0.29 degrees visual angle (Figure 3D), this means a decrease of roughly 25% in preferred eccentric position change from deep to superficial cortical portions. This result was the same for subjects whose anatomies were acquired at 0.5 mm

693resolution (slope coefficient: -0.064 degrees visual angle ($p < 0.001$)) and
694whose anatomies were acquired at a lower resolution (slope coefficients:
695-0.077 degrees visual angle ($p < 0.001$)). In sum, we found that changes in
696preferred eccentric position induced by spatial attention were larger in the
697deep cortical portions than in central and superficial cortical portions.
698

Figure 4

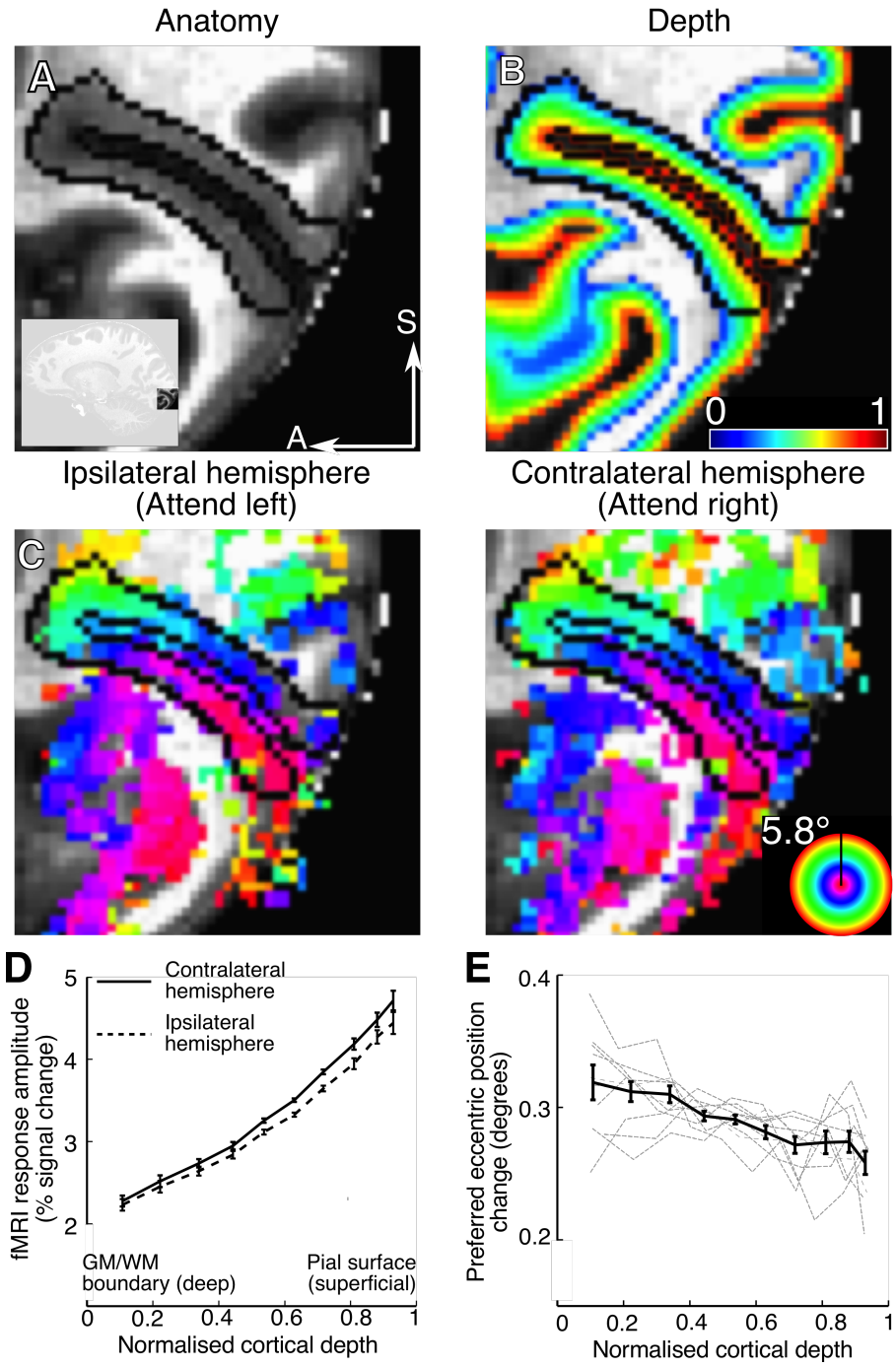

Figure 4 Preferred eccentric position changes as a function of cortical depth. A. Anatomical image for one of our subjects. The inset shows the entire sagittal slice. The black outline marks the borders of V1. The arrows indicate the anterior - posterior (A) and superior - inferior (S) axes. See Supplementary Figure 1 for all subjects. **B.** The same anatomical image overlaid with normalized cortical depth estimates. Zero/dark blue indicates the gray/white boundary whereas one/red indicates the cortical surface. **C.** The same anatomical image overlaid with preferred eccentric position estimates when the subject attended the ipsilateral

711(left panel) and contralateral (right panel) target. **D.** Averaged fMRI response amplitude
712across all subjects as a function of cortical depth when subjects attended the contralateral
713(solid line) and ipsilateral (dashed line) target. **E.** Preferred eccentric position changes as a
714function of cortical depth averaged across all subjects (solid black line), accounted for global
715difference in mean preferred eccentric position change. Thin gray lines represent the data
716from individual subjects, corrected for global difference in mean preferred eccentric position
717change. Error bars in D and E represent the standard error of the weighted mean across
718subjects per bin, determined by bootstrapping (1000 iterations). We find a significant negative
719slope across cortical depth, indicating larger preferred eccentric position changes in the deep
720cortical portion, near the gray matter/white matter (GM/WM) boundary.
721
722
723

3.3. Eye movements do not produce variation in pRF attraction across cortical depth

One factor that could potentially confound the results is subjects making involuntary eye movements towards the attended target during task performance (Figure 5A and Supplemental Figure 2). These eye movements towards the attended targets could potentially explain the preferred eccentric position changes.

First, we measured subjects' eye-movements in an identical setting outside the scanner. These measured eye movements recorded a bias in horizontal gaze position towards the attended target of 0.046 degrees visual angle per condition, yielding a total bias of 0.092 degrees between the two conditions. This gaze position bias would produce preferred eccentric position changes in the same direction as the attentional pRF attraction. However, the average attentional preferred eccentric position changes (0.29 degrees) are much larger. Furthermore, unlike attentional pRF attraction, the effects of eye-movements are similar across the visual hierarchy (Klein et al., 2014) and theoretically also across cortical depth.

To evaluate whether eye-movements can explain the preferred eccentricity change, we correlated subjects' average horizontal gaze position bias with the preferred eccentricity change in V1. This correlation is significant ($r = 0.66$, $p = 0.039$) but the effect is driven by one outlier (S10). S10's gaze position bias was almost twice the size of all other subjects. Removal of S10, removes the correlations between average gaze position bias and preferred eccentricity change ($r = 0.34$, $p = 0.37$). More importantly, the correlation of the average gaze position with the change of preferred eccentricity change across cortical depth is not significant with or without the outlier. Furthermore, removal of the outlier still maintains our main effect of significant variation of preferred eccentric position changes across cortical depth (slope coefficient ~ 0.06 degrees visual angle, $p = < 0.001$). Therefore, eye-movements can contribute to preferred eccentric position changes, but they do not produce the variation in preferred eccentric position changes across cortical depth in V1.

Furthermore, we conducted a control experiment as well as a simulation to evaluate whether eye-movements can explain the variation in preferred eccentric position across cortical depth. In the control experiment five subjects from the main experiment changed their gaze position between experimental runs rather than changing the location they attended. The total change in gaze position between conditions was 0.2 degrees, which is about twice the size of the gaze position bias between conditions measured prior to the scanning sessions. In the simulation, we introduced a change in gaze position to match the effect size of the attentional modulation (see section 2.10). Both measured and simulated eye movement-related preferred eccentric position changes did not have a significant slope across cortical depth (weighted linear regression, slope coefficients: 0.0086 ($p = 0.469$), Figure 5B solid gray line and 0.04283 ($p = 0.369$), Figure 5B dashed gray line, for measured and simulated data respectively). Thus, the main experiment but

not the control experiments show a significant variation across cortical depth. The latter is the case even if we restrict the main experiment to the subjects that participated in the control experiment.

Finally, the profile of fMRI response amplitude measured in the eye movement control experiment is very similar to the profile from the main attention experiment for the same subjects (Figure 5C, dashed black line and solid black line respectively). This demonstrates that the different profiles of preferred eccentric position change are not likely to be due to differences in fMRI response amplitude profiles between the two experiments.

In sum, the correlations with eye-position, control experiments, and simulations show that eye movements did not produce the cortical depth dependent effect on preferred eccentric position change we measured in the attention conditions.

Figure 5

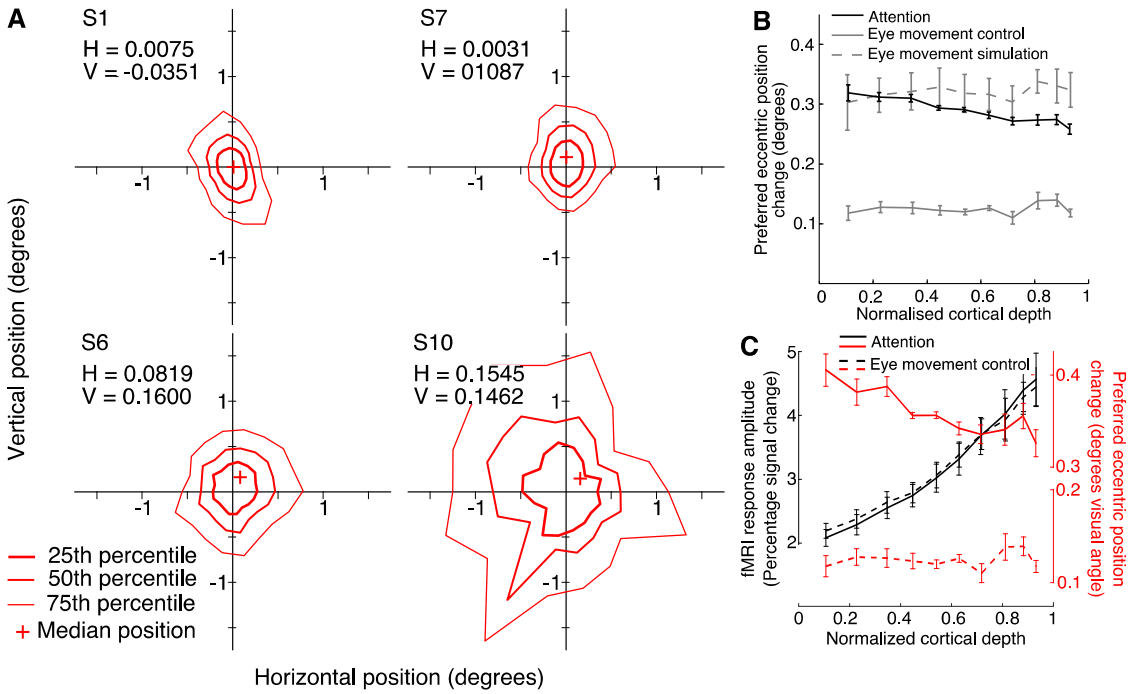

Figure 5. Subjects eye movements and their effect on the profile of preferred eccentric position change across cortical depth. A. Distribution of eye positions relative to the fixation point during task performance for two subjects with the smallest (S1 and S7) and largest (S6 and S10) gaze position bias. All gaze positions are arranged such that the attended location is always right of the center of the graph, at 6.3° visual angle. Red lines mark the 25th, 50th and 75th percentile of the gaze positions. The plus sign marks the median gaze position. See Supplementary Figure 2 for all subjects. **B.** Preferred eccentric position changes as a function of cortical depth produced by attention (solid black line, same data as in Figure 4E), measured (solid gray line), and simulated (dashed gray line) eye movements. Whereas attention produced a negative slope, eye movements did not. **C.** fMRI response amplitude (black lines) and preferred eccentric position changes (red lines), from the main attention experiment (solid lines) and eye movement control experiment (dashed lines) as a function of normalized cortical depth. The data from the main experiment is from the subjects that were also included in the eye movement control experiment. Despite the similar profiles of fMRI response amplitude for both experiments, the profiles of preferred eccentric position change are very different. All error bars represent the standard error of the weighted mean per bin, across subjects, determined by bootstrapping (1000 iterations).

3.4. pRF attraction is independent from fMRI response amplitude

Here we investigate whether changes in response amplitude are responsible for changes in pRF attraction. This is particularly relevant for cortical depth measurements as response amplitude varies with cortical depth (De Martino et al., 2013; Duvernoy, Delon, & Vannson, 1981).

FMRI response amplitude increased towards the cortical surface (Figure 4D) and this increase differed between the contralateral and ipsilateral hemispheres in the attention experiment (Figure 6A solid black line; weighted linear regression, slope coefficient: 0.26, $p < 0.001$). Thus, fMRI response amplitude changed in two important ways: 1. it increased from deep to superficial cortical portions, as expected from our GE sequence, and 2. this increase differed between contralateral and ipsilateral hemispheres. If the preferred eccentric position changes are related to fMRI response amplitude, these changes in response amplitude can be a potential confound.

In order to determine whether response amplitude is a potential confound, we assessed the relationship between preferred eccentric position changes and fMRI response amplitude. Preferred eccentric position changes across cortical depth are negatively correlated with fMRI response amplitude in the attention experiment, with averaged fMRI response amplitude increasing and preferred eccentric position change decreasing towards superficial portions (Figure 5C; solid lines). Thus, increased fMRI signals do not yield increased preferred position changes.

Alternatively, if low signal amplitudes would produce larger preferred position changes, we should measure a correlation between these two quantities in the eye movement control experiment as well. However, this is not the case. We do not find such a correlation ($p = 0.47$), despite the similarity in fMRI response profiles between the attention and control experiment (Figure 5C, black lines).

In addition, if preferred eccentric position changes are dependent on fMRI response amplitude, variation in response amplitude would bring about variation in preferred eccentric position changes as well. In this case, the difference in fMRI response increases between conditions in the attention experiment (Figure 6A) could underlie the profile of preferred eccentric position change (Figure 4E). If this were the case, the same would be true for the eye movement control experiment. However, we measured a similar difference in the increase in fMRI response amplitude across cortical depth in this experiment as we did in the attention experiment (Figure 6A; weighted linear regression, slope coefficient: 0.094, $p < 0.001$), Moreover, the control experiment revealed no variation in preferred eccentric position change (Figure 5B, gray lines).

Finally, we also simulated the effect of fMRI response amplitude on preferred eccentric position changes. We created two fMRI data sets and introduced a preferred eccentric position change between these two sets. Next, we computed the preferred eccentric position change between the sets for a range of response amplitudes (1 - 10 %-percent signal change) and added normal distributed, random noise to the data. We then bootstrapped

851(1000 iterations) the average preferred eccentric position change and the 95%
852confidence interval as a function of response amplitude. This simulation did
853not reveal a systematic bias of preferred eccentric position change as a
854function of fMRI response amplitude (Figure 6B).

855 In sum, fMRI response amplitude changed across cortical depth as
856expected, but also differed between conditions. However, this difference was
857not specific in the attention experiment, but also present in the eye movement
858control experiment. Importantly, neither our data nor our simulation support
859the possibility that these changes in fMRI response amplitude would produce
860the profile of preferred eccentric position changes as measured in the
861attention experiment.

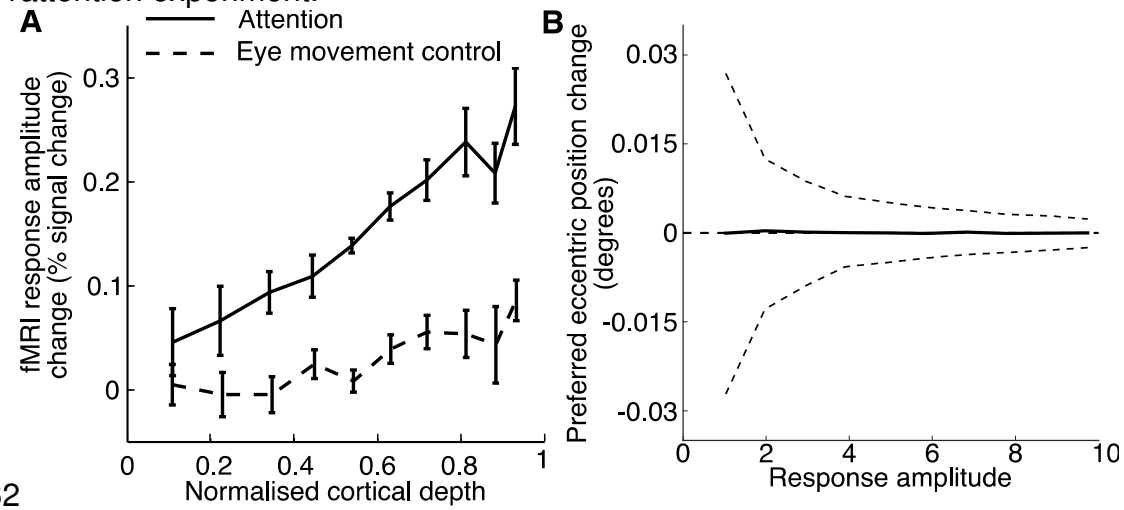

862

Figure 6. fMRI response amplitude changes. A. fMRI response amplitude change as function of cortical depth between contralateral and ipsilateral hemispheres for the attention experiment (solid line) and eye movement control experiment (dashed line). For both experiments, we find that response amplitude changes increase with cortical depth. **B.** Simulated preferred eccentric position change as a function of response amplitude. See section 3.4 for details. We bootstrapped the average preferred eccentric position change (solid line) and the 95% confidence interval (dashed lines) as a function of response amplitude. The preferred eccentric position changes are relative to the simulated change, 0.29 degrees, which is the same as the averaged preferred eccentric position change measured in the attention experiment (Figure 3D). Error bars in A represent the standard error of the weighted mean per bin, determined by bootstrapping (1000 iterations). This simulation reveals no systematic bias of preferred eccentric position change as a function of fMRI response amplitude.

4. Discussion

We used sub-millimeter, ultra-high field fMRI to assess attentional pRF attraction across cortical depth in human V1. We measured pRF attraction through changes in preferred eccentric position between two different locations at which voluntary spatial attention was directed. We extracted the profile of pRF attraction across cortical depth and found (1) pRF attraction at every cortical portion, and (2) strongest pRF attraction in the deep cortical portion, near the white/gray matter boundary, which decreased towards superficial portions. Control experiments demonstrate that eye movements cannot account for these results. Additionally, our approach focused on attentional modulations of preferred eccentric position, rather than fMRI response amplitude. As such, our results are not confounded by response amplitude variations across cortical depth resulting from the vascular properties of the cortex (De Martino et al., 2013; Duvernoy, Delon, & Vannson, 1981).

Combining computational models of attention with the known neuroanatomical organization of V1, we hypothesized that a feed forward mechanism would yield pRF attraction that does not vary across cortical depth (Figure 2D), and that a feedback mechanism would yield pRF attraction limited to either deep cortical portions, superficial cortical portions, or both (Figure 2E). Therefore, we interpret our results as providing evidence that a combination of feed forward and feedback mechanisms underlie pRF attraction in V1. We propose that the feedback component specifically targets deep cortical portions. We speculate that response modulations at the level of LGN produce pRF attraction in V1 central cortical portions (Felleman and Van Essen, 1991; McAdams and Maunsell, 1999; O'Connor et al., 2002; McAlonan et al., 2008). Following the flow of feed forward information across cortical depth, the pRF attraction in central cortical portions will be inherited by deep and superficial cortical portions (Briggs & Callaway, 2001; Callaway, 1998; Fitzpatrick, Lund, & Blasdel, 1985; Fracasso et al., 2016; Maunsell & Gibson, 1992; Self, Kerkoerle, Supèr, & Roelfsema, 2013; Usrey & Fitzpatrick, 1996; Yoshioka, Levitt, & Lund, 1994). The stronger pRF attraction in deep cortical portions cannot be explained by this feed forward mechanism. We suggest that this is the result of feedback processing. Likely sources of this feedback component are higher visual areas (Rockland and Pandya, 1979; Felleman and Van Essen, 1991).

We find a stronger pRF attraction in deeper cortical portions but not in superficial portions. This is an apparent contradiction with the presence of feedback afferents in superficial layers. There are several possible explanations for this. First, pRF attraction may reflect a specific type of feedback in which deep and superficial afferents may have different functional specializations. In recent years, a variety of cortical depth dependent effects on responses by feedback processing in general and endogenous attention specifically have been reported (Self et al., 2013; Muckli et al., 2015; Kok et al., 2016; Hembrook-Short et al., 2017; Kerkoerle et al., 2017; Nandy et al.,

2017; Self and Roelfsema, 2017). The specific targeting of deep cortical portions in pRF attraction is consistent with the overall picture that attentional modulation is selective and differs between cortical layers and cell types (Hembrook-Short et al., 2017; Nandy et al., 2017). Alternatively, attentional modulation across cortical depth may depend on the match between task demands and neural tuning properties. For example, Hembrook-Short and colleagues (2017) suggest that neurons with task-relevant properties -including contrast sensitivity- are more susceptible to attentional modulation. In this reasoning, neurons that were better suited to perform our contrast discrimination task may be attracted more. Consequently, if these neurons are more dominant in deeper cortical portions, this will result in stronger pRF attraction at those compartments.

One surprising aspect of our results is that pRF attraction is not integrated across cortical depth to yield the same amount of attraction at every depth. Apparently, pRFs are attracted to varying degrees across cortical depth. As a result, the spatial location that produces the strongest response changes from one cortical portion to the other. From the perspective of the computational aims in V1, this may seem counterproductive. Although we do not know what the computational consequences of this result are, we have reported a similar effect across the visual hierarchy (Klein et al., 2014). Here, pRF attraction varied between different visual field maps, apparently misaligning pRFs between different stages of the hierarchy.

Our results also show a pRF attraction in the central cortical portions, though weaker than in the deeper portions. This might appear to contradict our earlier statement that the observed pRF attraction is based on feedback connections. However, even if the neural feedback component would be limited to exclusively the deeper cortical portions, inherent spatial smoothing due to methodological (further discussed below) and analysis limitations would result in the gradual decrease of pRF attraction towards the surface that we find.

The attention field model predicts that pRF attraction is a function of pRF size and attention field size (equation 4). Specifically, larger pRFs will produce a stronger attraction. PRF size will vary with eccentricity (Hubel and Wiesel, 1962; Dumoulin and Wandell, 2008) and cortical depth (Fracasso et al., 2016). However, here we also showed that pRF attraction only varies with pRF size if the attention field directly interacts with the pRFs. Hierarchical processing will increase pRF size but not necessarily pRF attraction. Therefore, pRF attraction does not vary with pRF size if the attraction is inherited from earlier processing stages.

Nevertheless, one could ask whether we can measure pRF attraction as a function of pRF size. Unfortunately, we cannot. First, we focused on measuring pRF position by using an expanding ring stimulus, which is not suitable to reliably measure pRF size (Dumoulin and Wandell, 2008). Furthermore, due to the expanding ring stimulus, we cannot measure pRF positions outside the stimulus range. pRFs that are centered beyond our stimulus range, but still overlap with some of the stimulus' positions, will

appear to lie at the edge of our stimulus. This stimulus edge artifact complicates interpreting the profile of pRF attraction across eccentricity. Note that this stimulus artifact does not limit the overall pRF attraction that can be measured, which still allows us to draw conclusions about the cortical depth dependency of pRF attraction.

We find a large inter-subject variability of preferred eccentric position change across V1 (Figure 3D). This variability may have several origins. First, we know that pRF size typically varies between subjects by a factor of 2 to 3 (Harvey and Dumoulin, 2011). Therefore, variation in pRF size between subjects is likely to contribute to the variation in pRF attraction between subjects (Figure 2D). Second, variation in attention field size between subjects can produce variation in pRF attraction. Although we tailored task difficulty to yield similar performance across subjects, subjects may still display different task performance and effort. Finally, confounding factors, such as the variability in fixation bias can also contribute to the variability in measured pRF attraction - but not as a function of cortical depth.

We observed a decrease in pRF attraction from deep to superficial cortical portions, which we assessed assuming a linear relation between cortical depth and pRF attraction (Figure 4D). However, we hypothesized that a feedback contribution to pRF attraction specifically in deep cortical portions would manifest as a stronger pRF attraction in this portion followed by a reduced, constant attraction across central and superficial cortical portions (Figure 2E). We emphasize, however, that the aim of our hypothesized profiles was to give a qualitative overview of the expected results, not to predict the exact shape of pRF attraction across cortical depth. Methodological issues related to fMRI, such as partial volume effects and the BOLD spread function, will smooth the profile of pRF attraction and obscure its exact shape across cortical depth.

We also found that fMRI response amplitude changed in the attention experiment in two main ways: (1) it increased from deep to superficial cortical portions and (2) this increase differed between contralateral and ipsilateral hemispheres. The difference in increase between the contralateral and ipsilateral hemispheres seems to suggest that spatial attention increases fMRI responses near the attended location in a cortical depth dependent manner. However, as we found a similar profile for the eye movement control experiment, we cannot attribute this effect to spatial attention. Importantly, data from the eye movement control experiment and an additional simulation demonstrates that preferred eccentric position changes are independent from fMRI response amplitude. As such, changes in response amplitude do not underlie the profile of preferred eccentric position change in the attention experiment.

Finally, we have several reasons to exclude methodological issues concerning sub-millimeter fMRI, such as head motion and misalignment, as a possible explanation for our results. First, we collected all the experimental data for each subject in a single scanning session, with the left and right conditions alternating between scans. As such, the data from both attention

conditions are affected similarly by head motion and distortions of the functional volumes. Second, we used the same alignment between the functional and anatomical images for both left and right experimental conditions. Although we took great care to coregister the anatomical and functional volumes as accurately as possible (Figure 4 and Supplemental Figure 1), some coregistration inaccuracies may still be present. In that case, these inaccuracies would affect the data from both conditions equally. We point out that the fMRI response profile measured for the attention experiment is very similar to that of the control experiment (Figure 5C, black lines). This demonstrates that our approach is accurate enough to yield highly reproducible outcomes. Third, the data for the eye movement control experiment was acquired, pre-processed and analyzed in the same way as the data for the main experiment. However, in contrast to the main experiment, the control experiment did not reveal any significant variation of preferred eccentric position change across cortical depth, demonstrating that this variation is specific to the attention conditions in the main experiment.

5. Conclusions

In conclusion, we examined the influence of voluntary spatial attention on pRF positions across cortical depth in human V1. As we specifically focused on pRF position attraction, we avoided that our results would potentially be confounded by factors such as fMRI response amplitude differences across cortical depth. We observe pRF attraction in every cortical portion (deep, center and superficial) with the attraction being largest in the deep cortical portion, near the gray/white matter boundary. We speculate that this profile is best explained by a combination of a feed forward and a feedback mechanism underlying pRF attraction, with the feedback component operating stronger in deep cortical portions. Furthermore, our study highlights the utility of high-resolution functional imaging in providing insights in processes underlying attentional modulations of responses in early visual cortex.

Conflicts of Interest

The authors declare no competing financial interests.

Acknowledgements

This work was supported in part by the Netherlands Organization for Scientific Research (NWO) grant numbers (NWO 406-12-141 to B. P. K. and S. O. D.) and AMMODO KNAW Award (SD). The Spinoza Centre for Neuroimaging is a joint initiative of the University of Amsterdam, Academic Medical Center, VU University, VU medical center, Netherlands Institute for Neuroscience and the Royal Netherlands Academy for Arts and Sciences.

Appendix A. Supplementary figures

REFERENCES:

Bazin, P.L., Pham, D.L., 2007. Topology-preserving tissue classification of magnetic resonance brain images. IEEE Trans. Med. Imaging 26:487–496. doi:10.1109/TMI.2007.893283

Benevento, L.A., Rezak, M., 1976. The cortical projections of the inferior pulvinar and adjacent lateral pulvinar in the rhesus monkey (macaca mulatta): An autoradiographic study. Brain Res. 108:1–24. doi:10.1016/0006-8993(76)90160-8

Blasdel, G.G., Lund, J.S., 1983. Termination of afferent axons in macaque striate cortex. J. Neurosci. 3:1389–1413.

Bobier, B., Stewart, T.C., Eliasmith, C., 2014. A Unifying Mechanistic Model of Selective Attention in Spiking Neurons. PLoS Comput. Biol. 10. doi:10.1371/journal.pcbi.1003577

Brainard, D.H., 1997. The Psychophysics Toolbox. Spat. Vis. 10:433–436.

Briggs, F., Callaway, E.M., 2001. Layer-specific input to distinct cell types in layer 6 of monkey primary visual cortex. J. Neurosci. 21:3600–3608. doi:21/10/3600 [pii]

Callaway, E.M., 1998. Local Circuits in Primary Visual Cortex of the Macaque Monkey. Annu. Rev. Neurosci. 21:47–74. doi:10.1146/annurev.neuro.21.1.47

Compte, A., Wang, X.J., 2006. Tuning curve shift by attention modulation in cortical neurons: A computational study of its mechanisms. Cereb. Cortex 16:761–778. doi:10.1093/cercor/bhj021

Cox, R.W., 1996. AFNI: Software for Analysis and Visualization of Functional Magnetic Resonance Neuroimages. Comput. Biomed. Res. 29:162–173.

De Martino, F., Zimmermann, J., Muckli, L., Ugurbil, K., Yacoub, E., Goebel, R., 2013. Cortical Depth Dependent Functional Responses in Humans at 7T: Improved Specificity with 3D GRASE. PLoS One 8:e60514. doi:10.1371/journal.pone.0060514

Dumoulin, S.O., Fracasso, A., van der Zwaag, W., Siero, J.C.W., Petridou, N., 2017. Ultra-high field MRI: Advancing systems neuroscience towards mesoscopic human brain function. Neuroimage 0–1. doi:10.1016/j.neuroimage.2017.01.028

Dumoulin, S.O., Wandell, B.A., 2008. Population receptive field estimates in human visual cortex. Neuroimage 39:647–660. doi:10.1016/j.neuroimage.2007.09.034

Duvernoy, H.M., Delon, S., Vannson, J.L., 1981. Cortical blood vessels of the human brain. Brain Res. Bull. 7:519–579. doi:10.1016/0361-9230(81)90007-1

Engel, S.A., Glover, G.H., Wandell, B.A., 1997. Retinotopic organization in human visual cortex and the spatial precision of functional MRI. Cereb. Cortex 7:181–192. doi:10.1093/cercor/7.2.181

Engel, S.A., Rumelhart, B.A., Wandell, B.A., Lee, A.T., Glover, G.H., Chichilnisky, E.J., Shadlen, M.N., 1994. fMRI of human visual cortex. Nature 369:525.

Fedorov, A., Beichel, R., Kalpathy-Cramer, J., Finet, J., Fillion-Robin, J.C.,

1109 Pujol, S., Bauer, C., Jennings, D., Fennessy, F., Sonka, M., Buatti, J.,
1110 Aylward, S., Miller, J. V, Pieper, S., Kikinis, R., 2012. 3D Slicer as an
1111 image computing platform for the Quantitative Imaging Network. Magn.
1112 Reson. Imaging 30:1323–1341. doi:10.1016/j.mri.2012.05.001
1113Felleman, D.J., Van Essen, D.C., 1991. Distributed hierachical processing in
1114 the primate cerebral cortex. Cereb. Cortex 1:1–47.
1115Fitzpatrick, D., Lund, J.S., Blasdel, G.G., 1985. Intrinsic connections of
1116 macaque striate cortex: afferent and efferent connections of lamina 4C. J.
1117 Neurosci. 5:3329–3349.
1118Fracasso, A., Petridou, N., Dumoulin, S.O., 2016. Systematic variation of
1119 population receptive field properties across cortical depth in human visual
1120 cortex. Neuroimage 139:427–438. doi:10.1016/j.neuroimage.2016.06.048
1121Haak, K. van, Winawer, J., Harvey, B.M., Renken, R., Dumoulin, S.O.,
1122 Wandell, B.A., Cornelissen, F.W., 2013. Connective field modeling.
1123 Neuroimage 66:376–384.
1124Han, X., Pham, D.L., Tosun, D., Rettmann, M.E., Xu, C., Prince, J.L., 2004.
1125 CRUISE: Cortical reconstruction using implicit surface evolution.
1126 Neuroimage 23:997–1012. doi:10.1016/j.neuroimage.2004.06.043
1127Harvey, B.M., Dumoulin, S.O., 2011. The Relationship between Cortical
1128 Magnification Factor and Population Receptive Field Size in Human
1129 Visual Cortex: Constancies in Cortical Architecture. J. Neurosci.
1130 31:13604–13612. doi:10.1523/JNEUROSCI.2572-11.2011
1131Hembrook-Short, J.R., Mock, V.L., Briggs, F., 2017. Attentional Modulation of
1132 Neuronal Activity Depends on Neuronal Feature Selectivity. Curr. Biol.
1133 27:1–10. doi:10.1016/j.cub.2017.05.080
1134Herrmann, K., Montaser-Kouhsari, L., Carrasco, M., Heeger, D.J., 2010.
1135 When size matters: attention affects performance by contrast or response
1136 gain. Nat. Neurosci. 13:1554–1559. doi:10.1038/nn.2669
1137Hubel, D.H., Wiesel, T.N., 1974. Uniformity of monkey striate cortex: A
1138 parallel relationship between field size, scatter, and magnification factor.
1139 J. Comp. Neurol. 158:295–305. doi:10.1002/cne.901580305
1140Hubel, D.H., Wiesel, T.N., 1972. Laminar and columnar distribution of
1141 geniculo-cortical fibers in the macaque monkey. J. Comp. Neurol.
1142 146:421–50. doi:10.1002/cne.901460402
1143Hubel, D.H., Wiesel, T.N., 1962. Receptive fields, binocular interaction and
1144 functional architecture in the cat's visual cortex. J. Physiol. 160:106–154.
1145Kerkoerle, T. van., Self, M.W., Roelfsema, P.R., 2017. Effects of attention and
1146 working memory in the different layers of monkey primary visual cortex.
1147 Nat. Commun. 8:13804. doi:10.1038/ncomms13804
1148Klein, B.P., Harvey, B.M., Dumoulin, S.O., 2014. Attraction of Position
1149 Preference by Spatial Attention throughout Human Visual Cortex. Neuron
1150 84:227–237. doi:10.1016/j.neuron.2014.08.047
1151Klein, B.P., Paffen, C.L.E., te Pas, S.F., Dumoulin, S.O., 2016. Predicting bias
1152 in perceived position using attention field models. J. Vis. 16:1–15.
1153 doi:10.1167/16.7.15
1154Kok, P., Bains, L.J., Van Mourik, T., Norris, D.G., De Lange, F.P., 2016.

1155 Selective activation of the deep layers of the human primary visual cortex
1156 by top-down feedback. Curr. Biol. 26:371–376.
1157 doi:10.1016/j.cub.2015.12.038
1158Kumano, H., Uka, T., 2010. The Spatial Profile of Macaque MT Neurons Is
1159 Consistent With Gaussian Sampling of Logarithmically Coordinated
1160 Visual Representation. J. Neurophysiol. 104:61–75.
1161Lawrence, S.J.D., Formisano, E., Muckli, L., de Lange, F.P., 2017. Laminar
1162 fMRI: Applications for cognitive neuroscience. Neuroimage 1–7.
1163 doi:10.1016/j.neuroimage.2017.07.004
1164Lund, J.S., Lund, R.D., Hendrickson, A.E., Bunt, A.H., Fuchs, A.F., 1975. The
1165 origin of efferent pathways from the primary visual cortex, area 17, of the
1166 macaque monkey as shown by retrograde transport of horseradish
1167 peroxidase. J. Comp. Neurol. 164:287–303. doi:10.1002/cne.901640303
1168Marques, J.P., Kober, T., Krueger, G., van der Zwaag, W., Van de Moortele,
1169 P.F., Gruetter, R., 2010. MP2RAGE, a self bias-field corrected sequence
1170 for improved segmentation and T1-mapping at high field. Neuroimage
1171 49:1271–1281. doi:10.1016/j.neuroimage.2009.10.002
1172Maunsell, J.H., Gibson, J.R., 1992. Visual response latencies in striate cortex
1173 of the macaque monkey. J. Neurophysiol. 68:1332–1344.
1174 doi:10.1113/jphysiol.1962.sp006837
1175McAdams, C.J., Maunsell, J.H.R., 1999. Effects of Attention on Orientation-
1176 Tunnig Functions of Single Neurons in Macaque Cortical Area V4. J.
1177 Neurosci. 19:431–441.
1178McAlonan, K., Cavanaugh, J., Wurtz, R.H., 2008. Guarding the gateway to
1179 cortex with attention in visual thalamus. Nature 456:391–394.
1180Motter, B.C., 2009. Central V4 Receptive Fields Are Scaled by the V1 Cortical
1181 Magnification and Correspond to a Constant-Sized Sampling of the V1
1182 Surface. J. Neurosci. 29:5749–5757.
1183Muckli, L., De Martino, F., Vizioli, L., Petro, L.S., Smith, F.W., Ugurbil, K.,
1184 Goebel, R., Yacoub, E., 2015. Contextual Feedback to Superficial Layers
1185 of V1. Curr. Biol. 25:2690–2695. doi:10.1016/j.cub.2015.08.057
1186Nandy, A.S., Nassi, J.J., Reynolds, J.H., 2017. Laminar Organization of
1187 Attentional Modulation in Macaque Visual Area V4. Neuron 93:235–246.
1188 doi:10.1016/j.neuron.2016.11.029
1189O'Connor, D.H., Fukui, M.M., Pinsk, M.A., Kastner, S., 2002. Attention
1190 modulates responses in the human lateral geniculate nucleus. Nat.
1191 Neurosci. 5:1203–1209.
1192Pelli, D.G., 1997. The VideoToolbox software for visual psychophysics:
1193 Transforming numbers into movies. Spat. Vis. 10:437–442.
1194Petridou, N., Italiaander, M., van de Bank, B.L., Siero, J.C.W., Luijten, P.R.,
1195 Klomp, D.W.J., 2013. Pushing the limits of high-resolution functional MRI
1196 using a simple high-density multi-element coil design. NMR Biomed.
1197 26:65–73. doi:10.1002/nbm.2820
1198Reynolds, J.H., Heeger, D.J., 2009. The Normalization Model of Attention.
1199 Neuron 61:168–185. doi:10.1016/j.neuron.2009.01.002
1200Rockland, K.S., Pandya, D.N., 1979. Laminar origins and terminations of

1201 cortical connections of the occipital lobe in the rhesus monkey. Brain
1202 Res. 179:3–20. doi:10.1016/0006-8993(79)90485-2
1203Saad, Z.S., Glen, D.R., Chen, G., Beauchamp, M.S., Desai, R., Cox, R.W.,
1204 2009. Alignment using Local Pearson Correlation. Neuroimage 44:839–
1205 848. doi:10.1016/j.neuroimage.2008.09.037.A
1206Schira, M.M., Tyler, C.W., Breakspear, M., Spehar, B., 2009. The Foveal
1207 Confluence in Human Visual Cortex. J. Neurosci. 29:9050–9058.
1208 doi:10.1523/JNEUROSCI.1760-09.2009
1209Self, M.W., Roelfsema, P.R., 2017. Paying Attention to the Cortical Layers.
1210 Neuron 93:9–11. doi:10.1016/j.neuron.2016.12.032
1211Self, M.W., Van Kerkoerle, T., Goebel, R., Roelfsema, P.R., 2017.
1212 Benchmarking laminar fMRI: Neuronal spiking and synaptic activity
1213 during top-down and bottom-up processing in the different layers of
1214 cortex. doi:10.1016/j.neuroimage.2017.06.045
1215Self, M.W., Van Kerkoerle, T., Supè, H., Roelfsema, P.R., 2013. Article
1216 Distinct Roles of the Cortical Layers of Area V1 in Figure-Ground
1217 Segregation. Curr. Biol. 23:2121–2129. doi:10.1016/j.cub.2013.09.013
1218Sereno, M.I., Dale, a M., Reppas, J.B., Kwong, K.K., Belliveau, J.W., Brady,
1219 T.J., Rosen, B.R., Tootell, R.B.H., 1995. Borders of Multiple Visual Areas
1220 in Humans Revealed by Functional Magnetic Resonance Imaging
1221 Borders of Multiple Visual Areas in Humans Revealed by Functional
1222 Magnetic Resonance Imaging. Science (80-.). 268:889–893.
1223Shipp, S., 2003. The functional logic of cortico-pulvinar connections. Philos.
1224 Trans. R. Soc. Lond. B. Biol. Sci. 358:1605–1624. doi:10.1007/s00429-
1225 016-1250-9
1226Truong, T., Chen, B., Song, A.W., 2008. Integrated SENSE DTI with
1227 correction of susceptibility- and eddy current-induced geometric
1228 distortions 40:53–58. doi:10.1016/j.neuroimage.2007.12.001
1229Usrey, W.M., Fitzpatrick, D., 1996. Specificity in the axonal connections of
1230 layer VI neurons in tree shrew striate cortex: evidence for distinct
1231 granular and supragranular systems. J. Neurosci. 16:1203–1218.
1232Waehnert, M.D., Dinse, J., Weiss, M., Streicher, M.N., Waehnert, P., Geyer,
1233 S., Turner, R., Bazin, P.L., 2014. Anatomically motivated modeling of
1234 cortical laminae. Neuroimage 93:210–220.
1235 doi:10.1016/j.neuroimage.2013.03.078
1236Wandell, B.A., Chial, S., Backus, B.T., 2000. Visualization and measurement
1237 of the cortical surface. J. Cogn. Neurosci. 12:739–752.
1238 doi:10.1162/089892900562561
1239Wandell, B.A., Dumoulin, S.O., Brewer, A.A., 2007. Visual Field Maps in
1240 Human Cortex. Neuron 56:366–383. doi:10.1016/j.neuron.2007.10.012
1241Womelsdorf, T., Anton-Erxleben, K., Treue, S., 2008. Receptive Field Shift
1242 and Shrinkage in Macaque Middle Temporal Area through Attentional
1243 Gain Modulation. J. Neurosci. 28:8934–8944.
1244Yoshioka, T., Levitt, J.B., Lund, J.S., 1994. Independence and merger of
1245 thalamocortical channels within macaque monkey primary visual cortex:
1246 Anatomy of interlaminar projections. Vis. Neurosci. 11:467–489.

1247 doi:10.1017/S0952523800002406
1248